

## Optimisation of Doped Antimony Sulphide ( $\text{Sb}_2\text{S}_3$ ) Thin Films for Enhanced Device Applications

P.A. Nwofe<sup>1,\*</sup>, J.N. Chukwu<sup>2,†</sup>

<sup>1</sup> Department of Industrial Physics, Ebonyi State University, Abakaliki, P.M.B 53, Nigeria

<sup>2</sup> Department of Energy and Nuclear Engineering, La sapienza universita di Roma, Italy

(Received 03 July 2017; revised manuscript received 31 July 2017; published online 16 October 2017)

Energy scarcity is ubiquitous, and more acute in developing nations. Diversification of energy sources toward renewable energy is one of the world major approach in solving this problem. Thin film solar cells is universally recognized as one of the best way forward, thus investigation of low cost, non toxic inorganic materials for use in absorber and window layers in thin film photovoltaic solar cell devices will play a significant role in that regard. Thin films of antimony sulphide were grown using the solution growth technique. The films were doped with nickel impurities and annealed at annealing temperatures in the range 50 °C to 200 °C, with the annealing time fixed for 1 hour. The films were characterised using X-ray diffractometry to investigate the structural properties and UV-spectroscopy to investigate the optical properties, thus enabling to evaluate the optical constants (optical absorption coefficient, energy bandgap, refractive index, extinction coefficient, optical density, dielectric constants etc). The results from the structural analysis indicate that the films are mostly amorphous, and exhibited a polycrystalline form at an annealing temperature of 150 °C. The optical analysis show that the optical absorption coefficient were  $> 10^4 \text{ cm}^{-1}$ , the energy bandgap was direct with values in the range 2.26 eV to 2.52 eV. The results of the optical studies (direct energy bandgap, values of the energy bandgap and low resistivity) indicate that the films will be utilised as window layers in solar cell devices and in other optoelectronic applications.

**Keywords:** Energy scarcity, Semiconductor, Thin film solar cell, Antimony sulphide, Doping, Optoelectronics.

DOI: [10.21272/jnep.9\(5\).05007](https://doi.org/10.21272/jnep.9(5).05007)

PACS numbers: 88.40 –, 68.55.ag

### 1. INTRODUCTION

Energy and environmental sustainability are fundamental indicators of developed nations. Research in this regard has been ongoing for decades. The epileptic nature of power supply in third world nations is a common knowledge, added with little concern for environmental degradation. Some inorganic materials used in solar cell devices can constitute serious environmental hazards when not carefully disposed or recycled at the end-of-life, for example cadmium based devices. The potential hazards, and environmental concerns associated to the use of cadmium has been widely established in the literature [1-3]. Thin films of antimony sulphide have been widely used in various device applications including solar cells [4-12], photoconductors [13], television [14], and other optoelectronic devices [15]. It is noteworthy to mention that the constituent elements of antimony sulphide (Sb, S) are abundant and cheap, and also antimony (Sb) and sulphur (S) are more environmentally friendly compared to the other inorganic materials used in the more advanced thin film solar cells especially in CdTe solar devices. Antimony sulphide thin films can be deposited by a variety of low cost deposition techniques such as spray pyrolysis [16-17], chemical bath deposition [5-6, 13, 18] successive ionic layer adsorption and reaction (SILAR) [12], electro-deposition [19], hydrothermal synthesis [20-21], solvo-thermal synthesis [9, 22], and simple chemical route [23]. Thin films of  $\text{Sb}_2\text{S}_3$  has also been reported to be grown using thermal evaporation technique [8,14], and atomic layer deposition methods [10].

The aim of the present study is to investigate the

potentials of a low cost, non-toxic inorganic material for applications in optoelectronic devices especially in solar cell devices, hence the effect of post deposition annealing on the structural and optical properties of the doped layers are reported.

### 2. MATERIALS AND METHOD

#### 2.1 Substrate Preparation and Film Deposition

The soda lime glass substrate used for the deposition were thoroughly cleaned in an ultrasonic bath, and then dried. A 3.0g of antimony chloride was carefully measured and then included in a 10 ml of acetone in a beaker. A standard solution of sodium thiosulphate was prepared and the required volume was also added to the previous beaker and then stirred for 15 minutes to ensure uniform dissolution. The solution was then distributed into 6 separate beakers and labelled for easy identification. A standard solution of nickel was also prepared and 5 ml of it (0.3M) was then added to the respective 5 beakers (earlier labelled beakers), keeping one without the nickel to serve as control. The substrates were held vertically through a synthetic foam and deposition was allowed for 2 hours. The films were then removed and dried, and then placed in a furnace with annealing temperatures  $\leq 200$  °C, with the annealing time maintained for 1 hour.

#### 2.2 Characterisation

The films were characterised using X-ray diffractometry for the structural investigations and optical

\* [patricknwofe@gmail.com](mailto:patricknwofe@gmail.com)

† [callyjoe2002@yahoo.co.uk](mailto:callyjoe2002@yahoo.co.uk)

spectroscopy for the transmittance versus wavelength measurements. The optical measurements was done with a Unico-UV-2102PC spectrophotometer at a wavelength range of 300 nm to 1000 nm, while the structural characterisation was done using the PANalytical Xpert Pro Holland at a scan range of 10 to 90 degrees.

**3. RESULTS AND DISCUSSION**

The colour of the films were observed to be orange yellow by physical observation, and the films also adhered strongly to the substrates. The X-ray diffractogram of the layers are shown on Fig. 1. As indicated in Fig. 1, it is clear that the films exhibited a polycrystalline nature at an annealing temperatures  $\geq 50^\circ\text{C}$ . From the XRD analysis, it was observed that the films crystallized in the orthorhombic crystalline phase. The XRD pattern of the layers were found to be consistent with the ICDD-PDF:001-0538 (International centre for diffraction data powder diffraction file-001-0538). The observed results is in agreement with the literature [24].

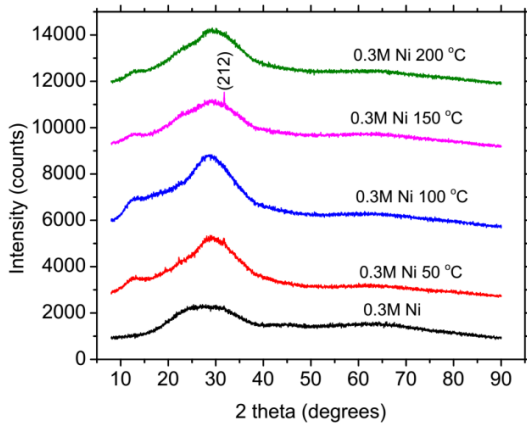


**Fig. 1** – XRD diffractograms of the layers at different annealing temperatures

Fig. 2 gives the plots of the transmittance with wavelength in the range 330 nm to 1000 nm. The transmittances of the films were typically  $< 80\%$  and exhibited an optimum for the films annealed at an annealing temperature of  $150^\circ\text{C}$ . The transmittance plots exhibited smooth profiles in all the layers as shown on Fig. 2, which points to the possibility of uniform doping in all the layers. The values of the transmittance obtained in the study is within the range reported by other research groups [25]. The effects of the post-deposition heat treatments was also significant in the transmittance plots as indicated in the shifts of the fundamental edge towards the higher wavelength. This behaviour was attributed to the modification in the valence and conduction band edge introduced by the nickel impurities. It is also possible that the difference in lattice constants of the dopants and host atoms are responsible for the observed phenomena.

Information extracted from the transmittance versus wavelength plots including relevant equation from the literature was used to deduce important optical constants such as the optical absorption coefficient ( $\alpha$ ), refractive index ( $n$ ) extinction coefficient ( $k$ ), dielectric

constants ( $\epsilon$ ), optical density, and the optical conductivity. The optical absorption coefficient was deduced using the relation [26];

$$\alpha = \frac{1}{d} \ln\left(\frac{100}{T\%}\right) \tag{1}$$

In equation 1,  $\alpha$  is the optical absorption coefficient,  $d$  is the film thickness, and  $T$  is the transmittance. From the analysis, it was observed that the values of  $\alpha$  were all  $> 10^4$  in all the layers. The behaviour exhibited by the plots of the variation of  $\alpha$  with the photon energy (not shown), is in agreement with the reports of other authors in the literature [27, 28].

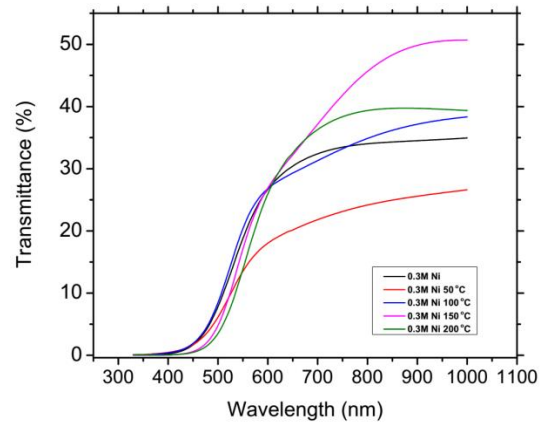


**Fig. 2** – Plots of transmittance vs. wavelength

Fig. 3 shows the variation of  $(\alpha hv)^2$  vs  $hv$  for the all the films at the different annealing conditions. It has been generally accepted that extrapolation of the linear portion of the graph of  $(\alpha hv)^2$  vs  $hv$  gives the energy bandgap of the material under study. The energy bandgap was calculated from the equation given in the literature [25, 29-30];

$$\alpha hv = B(hv - E_g)^n \tag{2}$$

where in equation (2),  $h$  is the Planck's constant,  $hv$  is the photon energy,  $B$  is an energy independent constant,

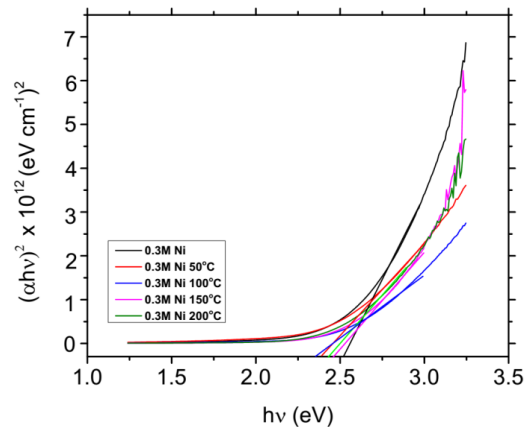


**Fig. 3** – Plots of  $(\alpha hv)^2$  vs  $hv$

$n$  is an index that characterises the optical absorption process,  $E_g$  is the energy bandgap and  $\alpha$  retains its meanings. The value of the index  $n$  is  $1/2$  for direct allowed transition, and  $3/2$  for direct forbidden transitions. The plots shown on Fig. 4 indicates that an extrapolation of the linear portion gives the energy bandgap in the range 2.26 eV to 2.52 eV. The results obtained for the energy bandgap is in line with the work of other authors [24-25, 29]. This range of values of the energy bandgap can be utilized in window layers for thin film solar cell applications.

Fig. 4 shows the relationship exhibited by the plots of the optical conductivity of the films with photon energy at the respective annealing conditions. The optical conductivity is directly related to the refractive index and optical absorption coefficient, and was evaluated using the relation given in the literature [24, 30-31];

$$\sigma = (\alpha n c) (4\pi)^{-1}. \quad (3)$$

In eq. 3,  $\sigma$  is the optical conductivity,  $\alpha$  retains its meanings,  $n$  is the refractive index, and  $c$  is the speed of light in vacuum. As expected, the optical conductivity of the layers were higher at shorter wavelength (higher photon energies) as these region of wavelengths are more absorbing. Also from the plots (Fig. 4), it was observed that the optical conductivities were lower at higher annealing temperatures.

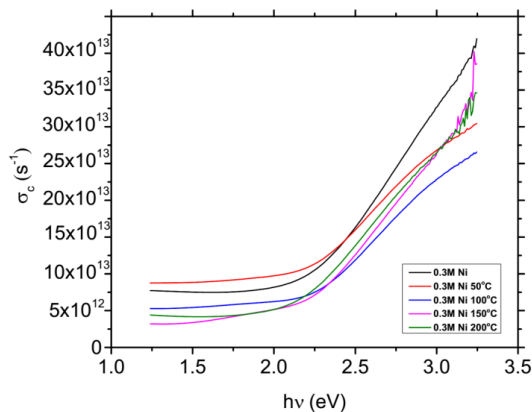


Fig. 4 – Plots of optical conductivity vs. photon energy

Fig. 5 shows the graph of the optical density with the photon energy. The optical density was calculated using the relation as contained in the literature [32], thus the optical density is given as;

$$\text{Optical density} = \alpha d. \quad (4)$$

In eq. 4,  $\alpha$  retains its meanings and  $d$  is the film thickness. The similarities in the behaviour of the plots of the optical densities with photon energy with that of the optical absorption coefficient with photon energy can be understood from the standpoint of the relationship in the equations (eqs. 3 and 4) used for the analysis. The optical densities were relatively higher at increased annealing temperatures. This behaviour could be attributed to the increase in the grain sizes due to the thermal treatments. An increase in the optical density, caused by a post deposition heat treatments

has been reported for other chalcogenides thin film independent of the deposition technique [32].

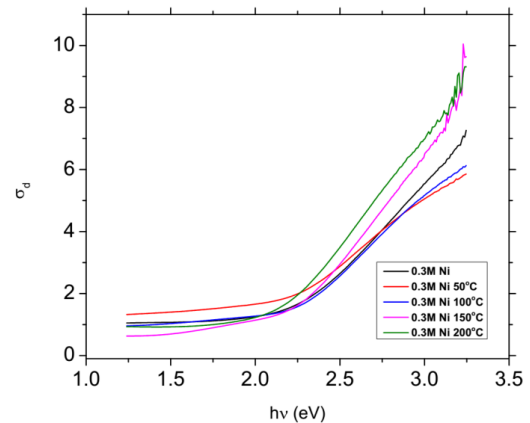


Fig. 5- Plots of optical density vs photon energy

Fig. 6 shows the change in refractive index with photon energy. According to the literature data (see, for example, [33]), the refractive index is related to the energy band gap hence the refractive index was calculated using the relation;

$$n^{-4} E_g = 77. \quad (5)$$

In eq. 5,  $n$  is the refractive index and  $E_g$  is the energy band gap. The refractive index decreased with increasing photon energies. The refractive index was in the range 2.2-2.8. These values are typically within the range suitable for various optoelectronic applications. The values of the refractive index obtained in the study is close to the reports of other research groups [24, 27-28].

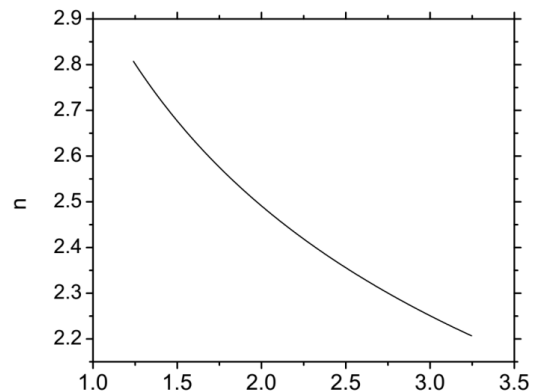


Fig. 6 – Plots of refractive index vs photon energy

#### 4. CONCLUSION

The study reports on the influence of post deposition heat treatment on the structural and optical properties of chemically deposited thin films of nickel-doped antimony sulphide. The post-deposition heat treatments modified the properties of the layers considerably. In particular the optical density increased with increasing annealing temperatures while the optical absorption coefficient were all  $> 10^5 \text{ cm}^{-1}$  in all the layers. The energy band gaps were direct, with values

in the range suitable for application in solar cell devices and in other optoelectronic applications. The values of the refractive index and the optical conductivities also suggest possible applications of the films in photoconductors.

## REFERENCES

1. S. Delbos, *EPJ Photovoltaic*, **3**, 35004 (2012).
2. N. Ali, A. Hussain, R. Ahmed, W.N. Wan Shamuri, A. Shaari, N. Ahmad, S.M. Abbas, *Appl. Phys. A* **122**, 23 (2016).
3. K.F. Abd-El-Rahman, A.A.A. Darwish, *Current Appl. Phys.* **11**, 1265 (2011).
4. J.A. Ramos Aquino, D.L. Rodriguez Vela, S. Shaji, D.A. Avellaneda, B. Krishnan, *phys. status solidi c* **13**, 24 (2016).
5. N. Ali, A. Hussain, R. Ahmed, W.W. Shamsuri, N.M. Abdel-Salam, R. Khenata, *Appl. Phys. A* **4**, 282 (2017).
6. S.C. Riha, A.A. Koegel, J.D. Emery, M.J. Pellin, A.B. Martinson, *ACS Appl. Mater. Interfaces* **9**, 4667 (2017).
7. L. Zheng, K. Jiang, J. Huang, Y. Zhang, B. Bao, X. Zhou, Y. Song, *J. Mater.Chem. A* **5**, 4791 (2017).
8. J. Escorcia-García, D. Becerra, M.T.S Nair, P.K. Nair, *Thin Solid Films* **569**, 28 (2014).
9. P. Sinsersuksakul, R. Chakraborty, S.B. Kim, S. M. Heald, T. Buonassisi, R.G. Gordon, *Chem. Mater.* **24**, 4556, (2012).
10. H. Wedemeyer, J. Michels, R. Chmielowski, S. Bourdais, T. Muto, M. Sugiura, G. Dennler, J. Bachmann, *Energ. Environ. Sci.* **6**, 67 (2013).
11. D. Pérez-Martínez, J.D. Gonzaga-Sánchez, F. Bray-Sánchez, G. Vázquez-García, J. Escorcia-García, M.T.S Nair, P.K. Nair, *Physica Status Solidi (RRL)-Rapid Research Letters*, **10**, 388 (2016).
12. S.U. Rahayu, C.L. Chou, N. Suriyawong, B.A. Aragaw, J.B. Shi, M.W. Lee, *APL Materials*, **4**, 116103 (2016).
13. S. Mushtaq, B. Ismail, M. Raheel, A. Zeb, *Nat. Sci.* **8**, 33 (2016).
14. M.A. Khan, A. Ahmed, N. Ali, T. Iqbal, A.A. Khan, M. Ullah, M. Shafique, *Am. J. Mater. Sci. & Engin.* **4**, 1 (2016).
15. A.D. DeAngelis, K.C. Kemp, N. Gaillard, K.S. Kim, *ACS Appl. Mater. Int.* **8**, 8445 (2016).
16. T. Rath, A.J. MacLachlan, M.D. Brown, S.A. Haque, *J Mater. Chem. A* **3**, 24155 (2015).
17. S. Shaji, L.V. Garcia, S.L. Loreda, B. Krishnan, J.A. Martinez, T.D. Roy, D.A. Avellaneda, *Appl. Surf. Sci.* **393**, 369 (2017).
18. M.J. Capistrán, M.T.S. Nair, P.K. Nair, *MRS Online Proceedings Library Archive* **7**, 1447 (2012).
19. R.A. Garcia, C.M. Avendaño, M Pal, F.P. Delgado, N.R. Mathews, *Mater. Sci. Semicon. Proc.* **44**, 91 (2016).
20. G. Xie, Z.P. Qiao, M.H. Zeng, X.M. Chen, S.L. Gao, *Crystal growth & design* **4**, 513 (2004).
21. G. Murtaza, M. Akhtar, M.A. Malik, P. O'Brien, N. Revaprasadu, *Mater. Sci. Semicon. Proc.* **40**, 643 (2015).
22. A. Hayakawa, M. Yukawa, T. Sagawa, *ECS Transactions*, **72**, 1 (2016).
23. W. Lou, M. Chen, X. Wang, W. Liu, *Chem. Mater.* **19**, 872 (2007).
24. Y. Yu, R.H. Wang, Q. Chen, L.M. Peng, *J. Phys. Chem. B* **110**, 13419 (2006).
25. H. Maghraoui-Meherzi, T.B. Nasr, N. Kamoun, M. Dachraoui, *Physica B* **405**, 3105 (2010).
26. C.O. Ozibo, P.A. Nwofe, P.E. Agbo, *World Appl. Sci. J.* **34**, 801 (2016).
27. B. Ismail, S. Mushtaq, A. Khan, *Chalcogenide Lett.* **11**, 45 (2014).
28. F. Aousgi, M. Kanzari, *Energy Procedia*, **10**, 313 (2011).
29. S. Srikanth, N. Suriyanarayanan, S. Prabahar, V. Balasubramanian, D. Kathirvel, *Adv. Appl. Sci. Res.* **2**, 95 (2011).
30. P.A. Nwofe, K.T. Reddy, R.W. Miles, *Adv. Mater. Res.* **602**, 1409 (2013).
31. P.E. Agbo, F.U. Nweke, P.A. Nwofe, C.N. Ukwu, *Int. J. Adv. Res.* **11**, 353 (2014).
32. C. Cifuentes, M. Botero, E. Romero, C. Calderon, G. Gordillo, *Brazilian J. Phys.* **36**, 1046 (2006).
33. Y. Wu, L. Assaud, C. Krysch, B. Capon, C. Detavernier, L. Santinacci, J. Bachmann, *J. Mater. Chem. A* **3**, 5971 (2015).

## ACKNOWLEDGEMENTS

Authors are grateful to the technical staff of Energy and Materials Research Institute, Akure, Nigeria, for the characterisation of the films.